

# Winter cold of eastern continental boundaries induced by warm ocean waters

Yohai Kaspi<sup>1</sup> & Tapio Schneider<sup>1</sup>

**In winter, northeastern North America and northeastern Asia are both colder than other regions at similar latitudes. This has been attributed to the effects of stationary weather systems set by elevated terrain (orography)<sup>1</sup>, and to a lack of maritime influences from the prevailing westerly winds<sup>2</sup>. However, the differences in extent and orography between the two continents suggest that further mechanisms are involved. Here we show that this anomalous winter cold can result in part from westward radiation of large-scale atmospheric waves—nearly stationary Rossby waves—generated by heating of the atmosphere over warm ocean waters. We demonstrate this mechanism using simulations with an idealized general circulation model<sup>3–5</sup>, with which we show that the extent of the cold region is controlled by properties of Rossby waves, such as their group velocity and its dependence on the planetary rotation rate. Our results show that warm ocean waters contribute to the contrast in mid-latitude winter temperatures between eastern and western continental boundaries not only by warming western boundaries, but also by cooling eastern boundaries.**

In middle latitudes, the eastern boundaries of Northern Hemisphere continents are colder than other regions at similar latitudes. Northeastern North America in winter is up to 20 K colder than similar latitudes in Europe, and northeastern Asia is similarly cold in comparison to northwestern North America (Fig. 1a). This anomalous cold has been attributed to several factors. The mean atmospheric flow in middle latitudes is westerly (eastward), so northeastern regions are farthest downstream from the warmer oceans, which may contribute to their coldness<sup>2</sup>. However, although Asia is much wider than North America, the longitudinal extent of the two continents' coldest regions is similar (Fig. 1a), so this cannot be the sole contributing factor. The pattern of stationary weather systems, such as the Icelandic low over the Atlantic and the Aleutian low over the Pacific, also contributes to the advection of cold polar air over the eastern continental regions (Fig. 1b). The positions and strength of these weather systems are controlled by orography and the distribution of diabatic heating in the atmosphere<sup>6,7</sup>. Orography has been posited as the principal factor controlling the temperature contrasts between eastern and western continental boundaries, in particular between North America and Europe, by generating stationary weather systems that drive warm and moist air towards Europe<sup>1</sup>. However, although the American and Asian regions of extreme cold polewards of 30° N have a similar structure (Fig. 1a), the North American and Asian orographies are very different. This suggests that yet further mechanisms contribute to the formation of the cold regions.

By sharp contrast, the western boundaries of oceans adjacent to the cold regions are characterized by strong, warm currents such as the Gulf Stream off the North American coast and the Kuroshio off the Asian coast. These boundary currents carry large amounts of heat polewards<sup>8</sup>, leading to large heat fluxes (mainly latent heat fluxes) from the warm oceans into the atmosphere (Fig. 1c). Here we show that atmospheric heating above warm ocean waters generates nearly stationary Rossby waves<sup>7,9</sup>, which cause an anomalously cold region immediately to the

west of the heating region. The size of this cold region is not set by the length scale of stationary waves<sup>9</sup>, but is controlled by the distance over which wave groups are radiated westwards before they dissipate.

To demonstrate this mechanism we use a three-dimensional general circulation model (GCM) with an active hydrological cycle<sup>3–5</sup>. The GCM is idealized, in that radiative transfer and moist convection are represented in a simplified manner, and processes not essential to the mechanism we study (for example, cloud-radiative feedbacks) are ignored. To represent heat fluxes from warm ocean waters, we added a localized ocean heat-flux convergence in the Northern Hemisphere; as a control, we added the same zonal-mean heat-flux convergence in the Southern Hemisphere, spread in a zonally symmetric fashion over all longitudes. The triangular heating region in the Northern Hemisphere (Fig. 2) roughly mimics the shape of the Asian and North American shorelines and the adjacent western boundary currents, with the western side of the triangle loosely representing the land–ocean boundary. The magnitude of the heat-flux convergence is set to resemble observed measurements (Fig. 1c), but the mechanism discussed here does not depend on details such as the magnitude or shape of the heating. See the Methods for details of the model.

To analyse systematically how heating leads to upstream cooling, we performed a series of simulations with planetary rotation rates between 0.25  $\Omega_e$  and 10  $\Omega_e$ , where  $\Omega_e$  is Earth's rotation rate. This allows us to discriminate between wave mechanisms that depend in different ways on the planetary rotation rate. We begin by looking at a simulation with Earth's rotation rate (Fig. 2, left column).

The localized surface heating induces a region of strong temperature gradients, and therefore strong baroclinicity, downstream (Supplementary Fig. 2). It also creates a region of strong atmospheric diabatic heating. Both factors contribute to the formation of a region of enhanced transient eddy kinetic energy downstream (Fig. 2a). Furthermore, the localized heating creates a stationary low-pressure system (cyclone) to its east and a stationary high-pressure system (anticyclone) to its west (Fig. 2d), resembling in structure and magnitude the pattern of stationary weather systems observed in nature (Fig. 1b). This pattern of stationary weather systems arises because, in the middle latitudes, atmospheric heating is primarily balanced by horizontal advection of cooler air, and this advection must be in approximate geostrophic balance with the pressure field<sup>10,11</sup>. The stationary circulation induced by localized heating causes equatorward advection of cold polar air towards the heating region and westward of it, and poleward advection of warm low-latitude air eastward of it (Fig. 2b).

The surface highs and lows are manifestations of stationary Rossby waves, which are induced by the localized heating<sup>6,7,9,10,12–14</sup>. These stationary waves can be described well by barotropic dynamics<sup>10</sup>, and can be seen clearly in the vertically averaged meridional velocity (Fig. 2c). The frequency of barotropic Rossby waves,  $\omega$ , is given by

$$\omega = \bar{u}k - \frac{\beta k}{k^2 + l^2} \quad (1)$$

where  $\beta$  is the planetary vorticity gradient,  $k$  is the zonal wave number,  $l$  is the meridional wave number and  $\bar{u}$  is the mean zonal velocity<sup>15</sup>. For

<sup>1</sup>California Institute of Technology, Pasadena, California 91125, USA.

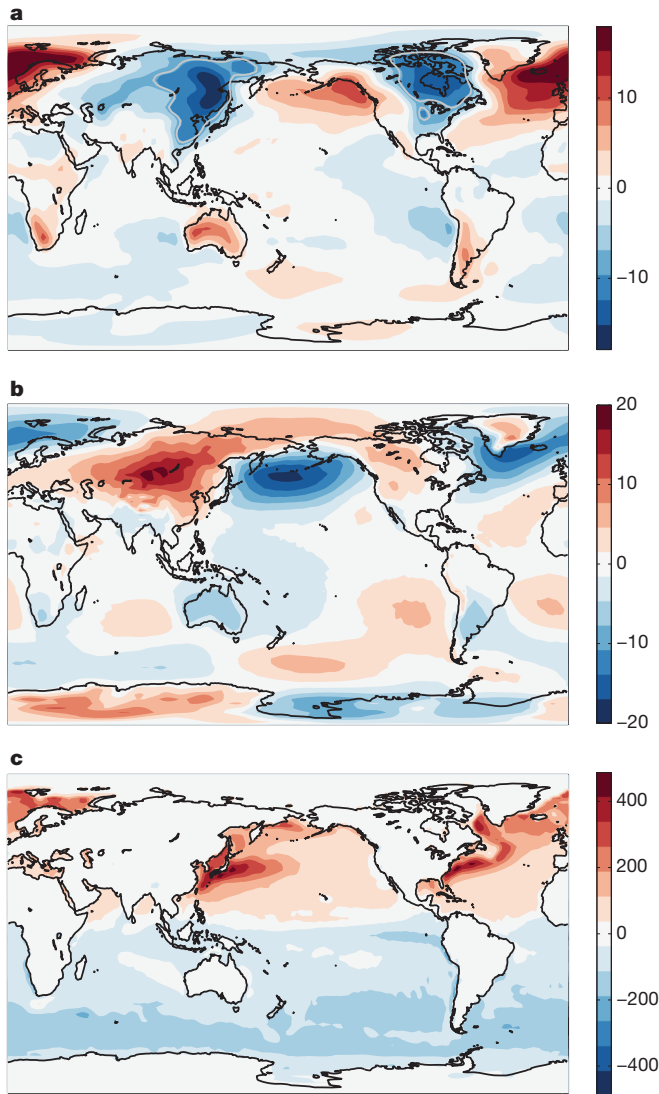


**Figure 1 | Observational data for Northern Hemisphere winter months (December–February), averaged between 1970 and 2009.** **a**, Surface-temperature deviation (K) from zonal mean ( $-8\text{ K}$  contour shown in grey, pointing to the similarity between the width of the cold regions in America and Asia). **b**, Interpolated sea-level pressure deviation from zonal mean (hPa). **c**, Implicit ocean heat-flux convergence ( $\text{W m}^{-2}$ ) given by  $Lh + Sh + LW - SW$ , where  $Lh$  is the latent heat flux,  $Sh$  is the sensible heat flux and  $LW$  and  $SW$  are the net upward longwave and downward shortwave radiative fluxes at the surface. This implicit ocean heat-flux convergence contains contributions from the actual ocean heat-flux convergence and the seasonal release of stored heat. (Based on reanalysis data from the US National Centers for Environmental Prediction<sup>22</sup>.)

isotropic waves ( $k = l$ ), this gives a length scale of  $\lambda = 2\pi(\bar{u}/\beta)^{1/2}$  when  $\omega = 0$  (that is, for stationary waves). For  $\Omega = \Omega_e$  and a typical mid-latitude value of  $\bar{u} \approx 20\text{ m s}^{-1}$ , this gives wavelengths of about 7,000 km, corresponding to about 4 wave crests over a latitude circle, similar to the length scales seen in nature and in the simulations (Figs 1b and 2c). One might thus infer that the longitudinal extent of the region of upstream cooling is set by the stationary Rossby wavelength.

However, when the planetary rotation rate is changed, it becomes clear that the extent of the region of upstream cooling is set by different dynamics. The extent of the cooling region increases with rotation rate (Fig. 2b), whereas the stationary Rossby wavelength decreases (Fig. 2c). Thus, it is not simply the phase of the stationary wave that controls the extent of the cold region upstream of the heating. As the rotation

rate increases, both the energy-containing length scale<sup>16</sup> and the stationary wavelength become smaller, whereas—counterintuitively—the cold region upstream expands.

The extent of the upstream cold region is controlled by the group dynamics of nearly stationary Rossby waves. Dispersive waves can have a non-zero group velocity ( $\vec{c}_g = \partial\omega/\partial(k, l)$ ) even when they are stationary<sup>17</sup>. The dispersion relation equation (1) implies the group velocity

$$\vec{c}_g = [c_{gx}, c_{gy}] = \left[ \bar{u} - \frac{\beta}{l^2}, 0 \right] \quad (2)$$

in the nearly stationary limit ( $\omega \rightarrow 0$ ) of zonally elongated waves ( $k \rightarrow 0$ )<sup>18,19</sup>. This zonal group velocity is westward for waves with a sufficiently large meridional scale, such that  $\bar{u} < \beta/l^2$ . Features such as an anticyclonic vorticity anomaly to the west of a localized heating can be then radiated farther westwards at this group velocity, forming a plume<sup>18–20</sup>. The extent of this plume is limited by the scale over which the nearly stationary Rossby wave groups propagate zonally. If the waves are damped on a time scale  $\tau$ , the plume can be expected to extend over a zonal scale  $L \sim c_{gx}\tau = (\bar{u} - \beta/l^2)\tau$ , which depends on  $\bar{u}$ ,  $\beta$  and the meridional scale of the localized heating,  $2\pi/l$ <sup>18,19</sup>. To the extent that variations in  $\bar{u}$  and  $\tau$  are relatively small, this length scale increases linearly with planetary rotation rate.

This is borne out in our simulations. The scale of the cold region upstream of the heating does indeed increase approximately linearly with rotation rate from  $0.5\Omega_e$  to  $10\Omega_e$  (Fig. 3). (The strength of the mid-tropospheric zonal flow  $\bar{u}$  varies by less than a factor of 2 in the range of rotation rates we have explored, and therefore does not strongly affect the approximately linear dependence between  $c_{gx}$  and  $\Omega$ .) For a meridional wave number  $l \approx 5$  corresponding to the scale of our heating region,  $\beta/l^2 \approx 28\text{ m s}^{-1}$  in middle latitudes for Earth's rotation rate, and this velocity increases with rotation rate. Therefore, for all cases in which  $\Omega \geq \Omega_e$  (for which  $\bar{u} \lesssim 20\text{ m s}^{-1}$  in the mid-troposphere), we have  $\bar{u} < \beta/l^2$ , and so the group velocity is westwards. The extent of the upstream cooling region is controlled by the westward radiation of nearly stationary Rossby wave groups, which decay over  $\tau$ . The variations in  $\bar{u}$  are weak relative to those in the rotation rate, so  $\tau$  can be inferred from the slope of the line of extent plotted against rotation rate (Fig. 3). It is of the order of days in our simulations. The damping time scale inferred from the regression of the extent of the cold region on the estimated group velocity of the waves varies by less than a factor of 2 as the rotation rate is varied, whereas the group velocity varies from about 10 to  $250\text{ m s}^{-1}$ . (An exact determination is difficult because it is unclear at precisely which level  $\bar{u}$  should be evaluated to obtain the group velocity.)

It happens that for Earth's rotation rate and the typical meridional scales of the heating regions over western boundary currents, the group velocity is such that the extent of the cold region upstream is similar to the length scale of a stationary Rossby wave. But the extent of the cold region is in fact controlled by different dynamics. Although downstream features of the circulation (for example, the eddy kinetic energy) may be controlled by stationary wave length scales<sup>21</sup>, the upstream cooling is controlled by the group velocity of nearly stationary, zonally elongated waves, as the simulations with different rotation rates show. Even when compared with a simulation without any extra heating (whether localized or spread out longitudinally in middle latitudes), the simulations with localized mid-latitude heating exhibit an anomalously cold region upstream.

Ref. 1 posited that winter temperature contrasts between mid-latitude eastern and western continental boundaries were controlled mostly by stationary weather systems caused by orography, as opposed to heating over oceans. However, this inference was based on eliminating all ocean heat transports in a GCM simulation, including tropical and subtropical transports, which resulted in widespread and large extratropical atmospheric cooling, with concomitant large atmospheric

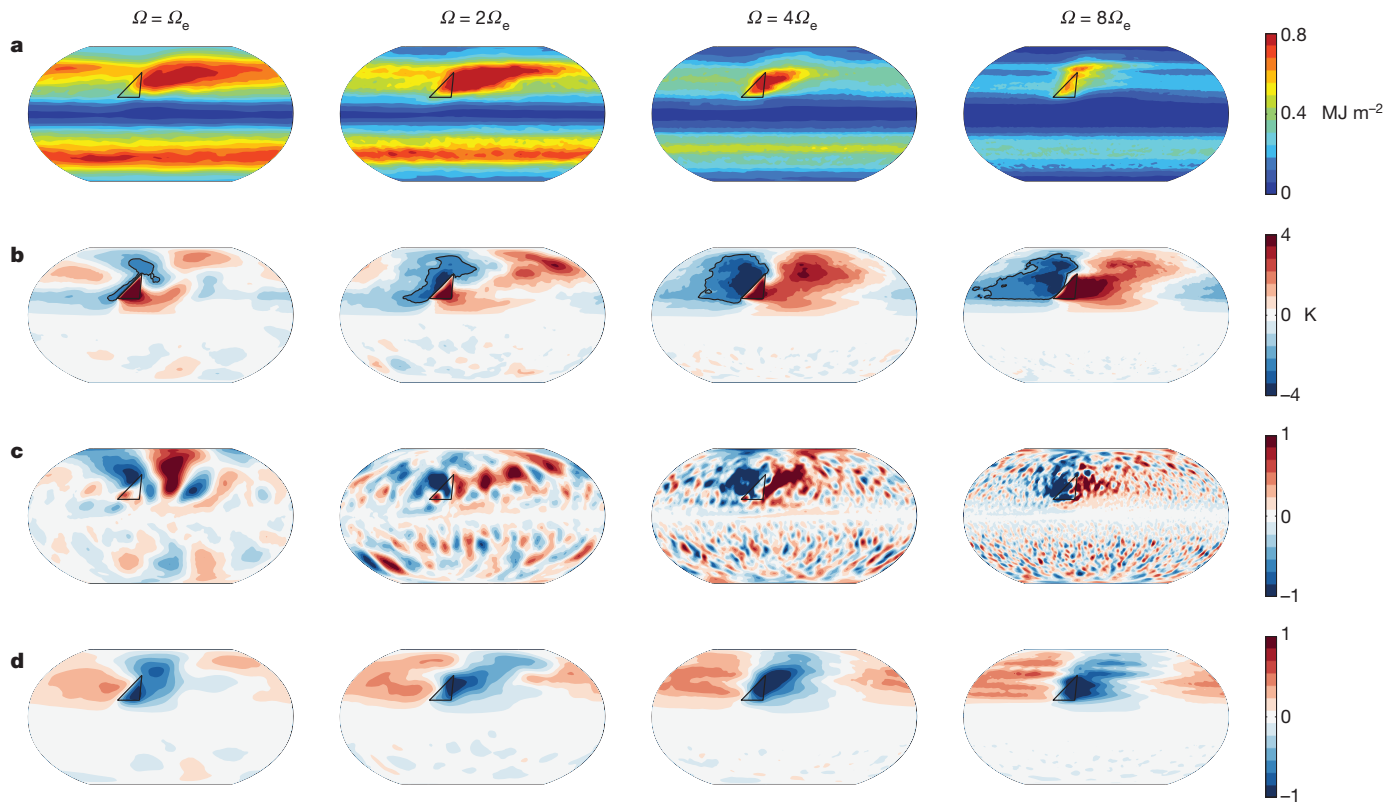


**Figure 2 | Time-averaged fields simulated with the idealized GCM for planetary rotation rates of  $\Omega_e$ ,  $2\Omega_e$ ,  $4\Omega_e$  and  $8\Omega_e$ .** **a**, Vertically integrated tropospheric transient eddy kinetic energy. **b**, Surface-temperature deviation from zonal mean. **c**, Vertically averaged tropospheric meridional velocity deviation from zonal mean. The units are non-dimensional, with 1 corresponding to  $2.5 \text{ m s}^{-1}$  (for  $\Omega_e$ ),  $1.5 \text{ m s}^{-1}$  ( $2\Omega_e$ ),  $0.75 \text{ m s}^{-1}$  ( $4\Omega_e$ ) and  $0.6 \text{ m s}^{-1}$  ( $8\Omega_e$ ), respectively. **d**, Surface-pressure deviation from zonal mean. The units are non-dimensional, with 1 corresponding to 10 hPa (for  $\Omega_e$ ), 15 hPa

( $2\Omega_e$ ), 20 hPa ( $4\Omega_e$ ) and 25 hPa ( $8\Omega_e$ ), respectively. In all figures, the heating region is marked with a triangle and has a uniform heat-flux convergence of  $500 \text{ W m}^{-2}$ , similar to observations. The upstream cooling increases linearly with the heat-flux convergence; see Supplementary Fig. 1. As the rotation rate increases, the eddy kinetic energy maximum becomes zonally more confined, whereas the upstream cold region expands. The stationary waves are evident in the meridional velocity (c).

circulation changes. This does not rule out the local importance of extratropical ocean heat fluxes for stationary weather systems.

We propose, then, that the anomalous winter cold of eastern continental boundaries can result at least in part from radiation of nearly stationary Rossby wave groups off the regions of large surface heat fluxes over the warm waters in oceanic western boundary currents. We have demonstrated this mechanism in the idealized GCM, with heat fluxes of similar magnitude to those observed over the western boundary currents, and with a climate similar to that of Earth in winter

(Supplementary Fig. 2). The GCM produces a stationary cyclone–anticyclone pair and a cold region upstream, with surface-pressure ( $\sim 10 \text{ hPa}$ ) and temperature ( $\sim 4 \text{ K}$ ) deviations from the zonal mean and from the mean over regions far downstream that are about half those observed on Earth (compare Figs 1 and 2). Thus, the Rossby-wave mechanism is probably quantitatively significant in producing the cold regions over eastern continental boundaries on Earth. Topography has already been shown to contribute<sup>1</sup>, and other factors ignored in the idealized GCM, such as land–ocean contrasts, effects of continentality and clouds probably also play a role. Nevertheless, the dynamics we have described are large-scale and robust. They provide a plausible answer to the question of why the eastern continental boundaries of both Asia and North America are so cold, and why the extent of the cold regions on both continents is similar.

## METHODS SUMMARY

The idealized GCM is based on the Flexible Modelling System of the US National Oceanic and Atmospheric Administration's Geophysical Fluid Dynamics Laboratory. It is a three-dimensional model of a spherical aquaplanet, and solves the primitive equations for an ideal-gas atmosphere<sup>3–5</sup>. We use a horizontal spectral resolution of T85 and 30 vertical levels. For simulations with planetary rotation rates  $\Omega$  greater than  $4\Omega_e$  we use the higher resolution of T127 to resolve the smaller energy-containing eddies. The lower boundary is a uniform slab ocean. Radiative transfer is represented by a two-stream grey radiation scheme. Moist convection is represented by a quasi-equilibrium convection scheme<sup>4</sup>, which relaxes temperatures towards a moist adiabat and water vapour towards a profile with fixed relative humidity relative to a moist adiabat. To damp small scales, strongly scale-selective hyperdiffusion is included in the vorticity, divergence and temperature equations.

Zonal asymmetries to initiate stationary waves are introduced by imposing a localized ocean heat-flux convergence in a triangular mid-latitude region. This is

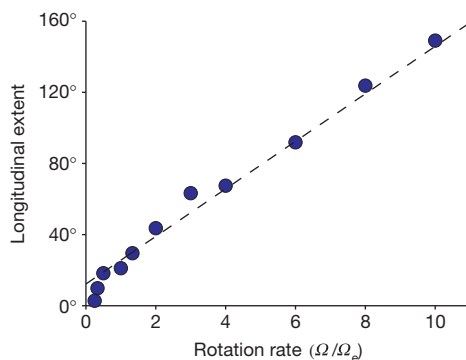


**Figure 3 | Extent of upstream cold region as a function of planetary rotation rate.** The extent of the upstream cold region is the longitudinal distance between the centre of the triangle and the westernmost extent of the bold  $-2 \text{ K}$  contour in Fig. 2b; the planetary rotation rate is given in multiples of  $\Omega_e$ . The dashed line represents the linear least-squares fit.

an idealized representation of the area of warm ocean waters and strong atmospheric diabatic heating in the Gulf Stream or Kuroshio western boundary currents. The magnitude of the heat flux convergence ( $500 \text{ W m}^{-2}$ ) is chosen to be similar to the observed heat fluxes (Fig. 1c). Our results do not depend qualitatively on the particular shape, size or magnitude of the imposed heat-flux convergence; the magnitude of the upstream cooling increases approximately linearly with the imposed heat-flux convergence (Supplementary Fig. 1). All simulation results presented are averages of flow fields sampled 4 times a day for at least 4 years, after a long spin-up period in which the GCM statistics reached a steady state.

**Full Methods** and any associated references are available in the online version of the paper at [www.nature.com/nature](http://www.nature.com/nature).

**Received 30 August 2010; accepted 10 February 2011.**

- Seager, R. *et al.* Is the Gulf Stream responsible for Europe's mild winters? *Q. J. R. Meteorol. Soc.* **128**, 2563–2586 (2002).
- Hartmann, D. L. *Global Physical Climatology* (Academic Press, 1994). Ch. 7.4.
- Frierson, D. M. W., Held, I. M. & Zurita-Gotor, P. A gray-radiation aquaplanet moist GCM. Part I: static stability and eddy scale. *J. Atmos. Sci.* **63**, 2548–2566 (2006).
- Frierson, D. M. W. The dynamics of idealized convection schemes and their effect on the zonally averaged tropical circulation. *J. Atmos. Sci.* **64**, 1959–1976 (2007).
- O'Gorman, P. A. & Schneider, T. The hydrological cycle over a wide range of climates simulated with an idealized GCM. *J. Clim.* **21**, 3815–3832 (2008).
- Held, I. M. in *Large-scale Dynamical Processes in the Atmosphere* (eds Hoskins, B. & Pearce, R.) 127–168 (1983).
- Held, I. M., Ting, M. & Wang, H. Northern winter stationary waves: theory and modeling. *J. Clim.* **15**, 2125–2144 (2002).
- Hsiung, J. Estimates of global oceanic meridional heat transport. *J. Phys. Oceanogr.* **15**, 1405–1413 (1985).
- Smagorinsky, J. The dynamical influence of large-scale heat sources and sinks on the quasi-stationary mean motions of the atmosphere. *Q. J. R. Meteorol. Soc.* **79**, 342–366 (1953).
- Hoskins, B. J. & Karoly, D. J. The steady linear response of a spherical atmosphere to thermal and orographic forcing. *J. Atmos. Sci.* **38**, 1179–1196 (1981).
- Held, I. M. & Ting, M. Orographic versus thermal forcing of stationary waves: the importance of the mean low-level wind. *J. Atmos. Sci.* **47**, 495–500 (1990).
- Lau, N. C. The observed structure of tropospheric stationary waves and the local balances of vorticity and heat. *J. Atmos. Sci.* **36**, 996–1016 (1979).
- Grose, W. L. & Hoskins, B. J. On the influence of orography on large-scale atmospheric flow. *J. Atmos. Sci.* **36**, 223–234 (1979).
- Cook, K. H. & Held, I. M. The stationary response to large-scale orography in a general circulation model and a linear model. *J. Atmos. Sci.* **49**, 525–539 (1992).
- Pedlosky, J. *Geophysical Fluid Dynamics* 2<sup>nd</sup> edn (Springer-Verlag, 1987).
- Schneider, T. & Walker, C. C. Self-organization of atmospheric macroturbulence into critical states of weak nonlinear eddy–eddy interactions. *J. Atmos. Sci.* **63**, 1569–1586 (2006).
- Lighthill, M. J. On waves generated in dispersive systems by travelling forcing effects, with applications to the dynamics of rotating fluids. *J. Fluid Mech.* **27**, 725–752 (1967).
- Rhines, P. B. in *Dynamics in Astrophysics and Geophysics* (ed. Lebovitz, N. R.) 3–58 (1983).
- Rhines, P. B. *Rosby Waves*, *Encyclopedia of Atmospheric Sciences* (Academic Press, 2002).
- Rhines, P. B. Jets and orography: idealized experiments with tip jets and Lighthill blocking. *J. Atmos. Sci.* **64**, 3627–3639 (2007).
- Kaspi, Y. & Schneider, T. Downstream self-destruction of storm tracks. *J. Atmos. Sci.* (in the press) (2011).
- Kalnay, E. *et al.* The NCEP/NCAR 40-year reanalysis project. *Bull. Am. Meteorol. Soc.* **77**, 437–470 (1996).

**Supplementary Information** is linked to the online version of the paper at [www.nature.com/nature](http://www.nature.com/nature).

**Acknowledgements** We thank D. Abbot, I. Eisenman, X. Levine and T. Merlis for comments. This research was supported by the National Oceanic and Atmospheric Administration Climate and Global Change Postdoctoral Fellowship administered by the University Corporation for Atmospheric Research (Y.K.), by a David and Lucile Packard Fellowship (T.S.), and by a grant from the National Science Foundation (AGS-1019211). The simulations were performed on the California Institute of Technology's Division of Geological and Planetary Sciences Dell cluster.

**Author Contributions** Y.K. and T.S. designed the study and wrote the paper; Y.K. performed the numerical simulations and data analyses.

**Author Information** Reprints and permissions information is available at [www.nature.com/reprints](http://www.nature.com/reprints). The authors declare no competing financial interests. Readers are welcome to comment on the online version of this article at [www.nature.com/nature](http://www.nature.com/nature). Correspondence and requests for materials should be addressed to Y.K. ([yohai@alum.mit.edu](mailto:yohai@alum.mit.edu)).

## METHODS

The idealized GCM is based on the Flexible Modelling System of the US National Oceanic and Atmospheric Agency's Geophysical Fluid Dynamics Laboratory. It is a three-dimensional model of a spherical aquaplanet, and solves the primitive equations for an ideal-gas atmosphere<sup>3–5</sup>. It does not take into account factors that are not essential to the mechanism, such as clouds, aerosols, sea-ice, water-vapour feedback and the diurnal and seasonal cycles.

**Resolution.** The GCM solves the hydrostatic primitive equations in vorticity-divergence form, using the spectral-transform method in the horizontal and finite differences in the vertical. The horizontal spectral resolution is T85 (corresponding to about  $1.4^\circ \times 1.4^\circ$  resolution of the transform grid). The vertical coordinate is  $\sigma = p/p_s$  (pressure  $p$  normalized by surface pressure  $p_s$ ), and has 30 discrete levels. For simulations with planetary rotation rates  $\Omega$  greater than  $4\Omega_e$ , we use the higher resolution of T127 to resolve the smaller energy-containing eddies.

**Radiative transfer.** Radiative transfer is represented by a two-stream grey radiation scheme with longwave and shortwave optical depths that depend only on latitude and pressure. The longwave optical thickness  $\tau$  is given by

$$\tau = [f_l \sigma + (1 - f_l) \sigma^4] [\tau_e + (\tau_p - \tau_e) \sin^2 \phi],$$

where  $\phi$  is latitude and  $f_l = 0.2$ . The linear and quadratic terms in  $\sigma$  roughly represent absorption by a well mixed absorber (with weight  $f_l$ ) and by water vapour (with weight  $1 - f_l$ ), respectively<sup>3,5</sup>. The term  $\tau_e$  represents the longwave optical thickness at the equator, and is equal to 4.8;  $\tau_p$  is the longwave optical thickness at the pole, and is 1.2. These are chosen to result roughly in a winter-hemisphere meridional temperature distribution. Solar radiative fluxes are imposed equally between hemispheres and are given by

$$S = \frac{S_0}{4} \left[ 1 + \frac{\Delta_s}{4} (1 - 3 \sin^2 \phi) \right] \exp(-\tau_s \sigma^2),$$

where  $S_0 = 1,360 \text{ W m}^{-2}$  is the solar constant,  $\Delta_s = 1.2$  controls the pole–equator insolation gradient and  $\tau_s = 0.22$  is the optical thickness for solar radiation.

**Moist convection and large-scale condensation.** Moist convection is represented by a quasi-equilibrium convection scheme<sup>4</sup>, which relaxes temperatures towards a moist adiabat with a time scale of 2 h, and water vapour towards a profile with fixed humidity of 70% relative to the moist adiabat, whenever a parcel lifted from the lowest model level is convectively unstable. Large-scale condensation removes water vapour from the atmosphere when the specific humidity on the grid scale exceeds saturation.

**Moist thermodynamics.** Water vapour is advected with a finite-volume scheme on the transform grid. A large-scale (grid-scale) condensation scheme ensures that the mean relative humidity in a grid cell does not exceed 100%. Only the vapour–liquid phase change is considered, and the saturation vapour pressure  $e_s$  is calculated from a simplified Clausius–Clapeyron relation given by

$$e_s(T) = e_0 \exp \left[ -\frac{L}{R_v} \left( \frac{1}{T} - \frac{1}{T_0} \right) \right],$$

where  $R_v = 461.5 \text{ J kg}^{-1} \text{ K}^{-1}$  is the gas constant for water vapour,  $L = 2.5 \times 10^6 \text{ J kg}^{-1}$  is a fixed latent heat of vaporization, and  $e_0 = 610.78 \text{ Pa}$  is the vapour pressure and  $T_0 = 273.16 \text{ K}$  the temperature at the triple point of water.

**Boundary layer.** The lower boundary of the GCM is uniform and water covered, with an albedo of 0.38. A planetary boundary-layer scheme with Monin–Obukhov surface fluxes, which depend on the stability of the boundary layer, links atmospheric dynamics to surface fluxes of momentum, latent heat and sensible heat. The roughness length for momentum, moisture and heat fluxes is  $1 \times 10^{-3} \text{ m}$ , and an additive gustiness term of  $1 \text{ m s}^{-1}$  is added to surface velocities in bulk aerodynamic formulae to represent subgrid-scale wind fluctuations. These values allow us to obtain energy fluxes and a climate similar to Earth's in the aquaplanet setting of our simulations. Our results are not very sensitive to the choice of these parameters.

**Subgrid-scale dissipation.** Above the boundary layer, horizontal  $\nabla^8$  hyperdiffusion in the vorticity, divergence and temperature equations is the only dissipative process. The hyperdiffusion coefficient is chosen to give a damping time scale of 12 h at the smallest resolved scale.

**Surface energy balance.** The surface temperature evolves according to the surface energy balance of a homogeneous slab, with temperature tendencies balanced by insolation, thermal radiative fluxes and the surface fluxes of sensible heat and latent heat. The precise value of the heat capacity (or thickness) of the slab does not substantially affect our results, which are for statistically steady states. In our simulations, the slab has a heat capacity corresponding to a 1-m layer of water.

**Spin-up.** All simulations have been spun-up to statistically steady state for at least 3,000 simulation days. The results presented here have been averaged over at least 4 years of simulation time beyond spin-up, and are all in a statistically steady state.

**Zonal Asymmetries.** Zonal asymmetries are introduced by imposing a localized heat-flux convergence in a triangular mid-latitude region. This is an idealized representation of the area of warm ocean waters and strong atmospheric heating in the Gulf Stream or Kuroshio western boundary currents. The localized heating is applied between latitudes  $25^\circ \text{ N}$  and  $50^\circ \text{ N}$ . The magnitude of the heat-flux convergence ( $500 \text{ W m}^{-2}$ ) is chosen to be similar to the observed heat fluxes from the surface (Fig. 1c). Our results do not depend qualitatively on the particular shape, size or magnitude of the imposed heat-flux convergence. The upstream cooling increases approximately linearly with the magnitude of the heating (Supplementary Fig. 1). As a control case, we impose in the Southern Hemisphere a heat-flux convergence that is equal in the zonal mean to that in the Northern Hemisphere, but is spread zonally symmetrically over all longitudes. (The deviations from the local zonal mean in the Northern Hemisphere shown in Fig. 2 are very similar to the corresponding deviations from the Southern Hemisphere zonal mean.)